A Nonfitting Method Using a Spatial Sine Window Transform for Inhomogeneous Effective-Diffusion Measurements by FRAP

Darya Y. Orlova,[†‡] Eva Bártová,[†] Valeri P. Maltsev,[‡§] Stanislav Kozubek,[†] and Andrei V. Chernyshev[‡§*]
[†]Institute of Biophysics, Academy of Sciences of the Czech Republic, Brno, Czech Republic; [‡]Institute of Chemical Kinetics and Combustion, Novosibirsk, Russia; and [§]Novosibirsk State University, Novosibirsk, Russia

ABSTRACT Determining averaged effective diffusion constants from experimental measurements of fluorescent proteins in an inhomogeneous medium in the presence of ligand-receptor interactions poses problems of analytical tractability. Here, we introduced a nonfitting method to evaluate the averaged effective diffusion coefficient of a region of interest (which may include a whole nucleus) by mathematical processing of the entire cellular two-dimensional spatial pattern of recovered fluorescence. Spatially and temporally resolved measurements of protein transport inside cells were obtained using the fluorescence recovery after photobleaching technique. Two-dimensional images of fluorescence patterns were collected by laser-scanning confocal microscopy. The method was demonstrated by applying it to an estimation of the mobility of green fluorescent protein-tagged heterochromatin protein 1 in the nuclei of living mouse embryonic fibroblasts. This approach does not require the mathematical solution of a corresponding system of diffusion-reaction equations that is typical of conventional fluorescence recovery after photobleaching data processing, and is most useful for investigating highly inhomogeneous areas, such as cell nuclei, which contain many protein foci and chromatin domains.

INTRODUCTION

Fluorescence recovery after photobleaching (FRAP) has become a widely used approach for investigating the behavior of proteins in living cells (1) providing the ability to target concentrated laser illumination onto a user-defined region of bleach (ROB) in order to observe the fluorescence intensity averaged over a region of interest (ROI). FRAP has now been adopted as a common technique for studying almost all aspects of cell biology, including chromatin structure (2), transcription (3), mRNA mobility (4), protein recycling (5), signal transduction (6), cytoskeletal dynamics (7), vesicle transport (8), cell adhesion (9), and mitosis (10).

Although the photobleaching method has been in use since the 1970s (11–13), renewed interest in its application reflects the advent of fluorescent protein tags, such as green fluorescent protein (GFP) fusion proteins (14). GFP is well suited for photobleaching studies (15,16). It is a bright, stable, nontoxic fluorophore that does not bleach significantly under low-intensity imaging conditions. When illuminated at high intensity, GFP bleaches irreversibly without damaging intracellular structures (15–18). An important feature of GFP is the ability of cells to express it themselves. GFP fusion proteins can target intracellular organellar regions not usually accessible to probes microinjected into the cytoplasm. This is particularly true for the cell nucleus, which has only recently been the subject of endogenous protein mobility studies (19). FRAP experiments require rapid switching between a low-intensity imaging mode and a high-intensity bleaching mode, during which the bleached region is positioned precisely. A laser-scanning confocal microscope is generally suitable for such applications without additional modifications (20). Thus, the recent advent and availability of both fluorescent protein technology and confocal microscopy have led to a resurgence in the use of FRAP for studying protein mobility in the interior of living cells (21).

In practice, FRAP results are often analyzed qualitatively to determine whether protein mobility is rapid or slow, whether binding interactions are present, whether an immobile fraction exists, or how a particular treatment affects these properties (1). There are also empirical FRAP methods (22,23), which are based on the idea that if each sample is treated precisely the same (e.g., same bleach intensity, bleach time, and bleach geometry), a relative diffusion coefficient can be obtained by comparing the recovery-half-times. In practice, however, these methods may give misleading interpretations of recovery curves due to the complexity of the photobleaching process in a sample, especially in inhomogeneous systems.

Quantitative analyses of FRAP data are usually based on fitting the experimental fluorescence recovery curve to a particular FRAP model. Therefore, to ensure that the parameters obtained are valid, it is important that experiments be carried out according to the FRAP theory used. Several mathematical models have been developed to better understand the underlying processes; ensure the accuracy of a qualitative interpretation; and extract quantitative parameters from a FRAP curve, such as association and dissociation constants, distribution of a protein between mobile and immobilized pools, and the effective diffusion coefficient of the molecule under study.

Submitted August 15, 2010, and accepted for publication November 30, 2010.

*Correspondence: chern@kinetics.nsc.ru

Editor: Anne Kenworthy.

© 2011 by the Biophysical Society
0006-3495/11/01/0507/10 $2.00

doi: 10.1016/j.bpj.2010.11.080

Among the analytical issues that have been addressed are the following:

- Two-dimensional diffusion and one-dimensional flow for Gaussian and uniform-spot photobleaching, by Axelrod et al. (12);
- FRAP for a Gaussian spot in the case of second-order photobleaching kinetics by Bjarneson and Petersen (24);
- A three-dimensional extension of the Gaussian spot, by Blonk et al. (25), and a similar three-dimensional extension of the uniform spot, derived by Braeckmans et al. (26);
- A numerical approach for two-dimensional FRAP, by Lopez et al. (27) and Wedekind et al. (28), and later in three dimensions, by Kubitscheck et al. (29);
- A method for analyzing a distribution of diffusion coefficients, by Periasamy and Verkman (30);
- A FRAP technique using continuous spot photobleaching to allow calculation of dissociation and residence times at binding sites in addition to determination of diffusion coefficients, by Wachsmuth et al. (31);
- A model to determine molecular kinetic rate constants under nonsteady-state conditions, by Lele and Ingber (32); and
- A formula for FRAP for the binding diffusion model in the form of a closed-form analytic expression, by Kang and Kenworthy (33).

The foregoing methods are applicable to conventional FRAP using a focused laser spot. Conventional FRAP has become a very useful tool for measuring translational mobility on a microscopic scale. However, because conventional FRAP measures the total fluorescence intensity of the bleached region, no spatial information can be directly obtained. Without such spatial resolution, it is impossible to analyze variations in the two-dimensional distributions of a fluorophore during the recovery process. In video-FRAP, a modification of this technique, a series of images is acquired after photobleaching, allowing the spatial character of the recovery to be determined. A two-dimensional spatial Fourier transform analysis of the images after photobleaching that utilizes all of the available image data to determine mobility coefficients was presented by Tsay and Jacobson (34) and developed further by Berk et al. (35). The Fourier method has the advantage of being independent of bleaching kinetics and possible recovery during bleaching.

An additional advantage is that the bleaching geometry is completely arbitrary. A fundamental feature of the Fourier method is that the effective diffusion coefficient is obtained without taking association and dissociation constants into consideration. This feature does not reduce the attractiveness of the method, because until recently the major use of the FRAP technique has been to measure the translational motion of molecular components in various condensed media. But such experiments should be carried out within the confines of the diffusion-dominant scenario, in which the binding site association time is much faster than the time required to diffuse across the bleached area.

Therefore, as has been previously noted (40), the applicability of the diffusion-dominant model in a particular case depends on the size of the fluorescence averaging region (ROI). On the other hand, increasing the size of the fluorescence averaging region (which increases the time required to diffuse across the region) expands the applicability of the diffusion model to samples with slower binding rates. The Fourier method is very tidy in theory, but unfortunately is very noise-sensitive. To reduce the noise level, it has been suggested that the lowest spatial frequency of the Fourier transform be used (35).

It has recently been shown (37) that the use of the Hankel transform instead of the Fourier transform reduces noise, primarily due to compensation for temporal variations in the data. However, both the Fourier and the Hankel methods were originally developed for homogeneous media. Strictly speaking, the application of these methods to highly inhomogeneous samples is not fundamentally derived from master equations. For example, under homogenous-media assumptions, transform intensities obtained using these methods exhibit an exponential change over time, a temporal behavior that is essentially different from that of inhomogeneous media. This circumstance may lead to misinterpretation of the effective diffusion coefficients obtained for inhomogeneous samples.

It should be noted that most, if not all, quantitative FRAP methods require the use of a particular mathematical solution of corresponding differential (master) equations in order to evaluate parameters (e.g., diffusion coefficient). This substantially reduces the efficiency of such methods in highly inhomogeneous media, where the mathematical solution is impossible to derive in a general case of unknown spatial distribution of binding sites.

In this article, we present a nonfitting FRAP method that takes into account the inhomogeneity of the sample. In the method, inside of the FRAP video-frame, one selects a rectangular ROI, which may be different from the ROB, and the effective diffusion coefficient averaged over the ROI is evaluated from spatially and temporally resolved video-FRAP measurements. The advantage of the method is that it does not require a mathematical solution of corresponding master equations in the case of the diffusion dominant scenario. The method is independent of bleaching geometry, bleaching kinetics, possible recovery during bleaching, and the spatial distribution of binding sites. In the method, a large area of the ROI is used, expanding the effective diffusion approach to reactions that are much slower than those amenable to diffusion dominant analysis using a conventional small ROI.

An additional advantage is that the method is less sensitive to noise in the FRAP data than the Fourier method,

because even the Fourier transform with the lowest spatial frequency has a spatial frequency that is higher (approximately twofold) than that of the proposed sine window transform. The method is most useful for the investigation of highly inhomogeneous areas, such as cell nuclei. It should be noted that the use of the sine window transform obviates the need to account for nonzero spatial derivatives of the fluorescence intensity on the boundary of the rectangular ROI (which are difficult to measure or calculate in an inhomogeneous media), as is turned out for the general Fourier window transform.

The method was validated for the determination (and comparison with known literature data) of the diffusion coefficient of fluorescein isothiocyanate (FITC)-labeled human serum albumin (FITC-HSA) diffusion in the glycerol/water mixture (80% w/w). The applicability of the method for inhomogeneous systems was demonstrated for the evaluation (and comparison with known literature data) of the mobility of GFP-tagged heterochromatin protein 1 (GFP-HP1) in the nuclei of living cells (mouse embryonic fibroblasts).

MATERIALS AND METHODS

Plasmids

The plasmids encoding GFP-HP1α, GFP-HP1β, and GFP-HP1γ were a generous gift from Dr. Tom Misteli (National Institutes of Health, Bethesda, MD). Constructs were used to transform competent *E. coli* DH5α, and plasmid DNA was isolated using a Qiagen Large-Construct kit (catalogue No. 12462; Qiagen, Bio-Consult, Bozejovická, Czech Republic).

Cell culture and transfection

Mouse embryonic fibroblasts (MEFs) from wild-type (wt) mice and mice deficient for both histone methyltransferases (HMTs) Suv39h1 and Suv39h2 (*Suv39h1/2*$^{-/-}$ mice) were used. Immortalized *Suv39h1/2*$^{-/-}$ MEFs originated in the laboratory of Prof. Thomas Jenuwein at the Max-Planck Institute of Immunobiology, Freiburg, Germany. Immortalized MEFs from mice homozygous null for the A-type lamin gene (*Lmna*$^{-/-}$ mice) and corresponding wt MEFs were a generous gift from Dr. Teresa Sullivan and Prof. Collin L. Stewart. MEFs were grown to 70% confluence on microscope coverslips in high glucose D-MEM medium supplemented with 10% fetal calf serum, penicillin (100 U/mL), and streptomycin (100 μg/mL) in humidified air containing 5% CO_2, at 37°C.

For measurements of protein motion, cells were transfected with an expression vector containing GFP-tagged HP1 (α, β, γ) using the transfection reagent METAFECTENE EASY (Biontex, Munich, Germany), as described by the manufacturer. The cells were subsequently incubated for 20 h at 37°C in a 5% CO_2 atmosphere to allow for HP1-GFP expression. The medium was then replaced with fresh medium.

These studies were also supplemented by experiments analyzing the effect of histone deacetylase inhibition on the structure and dynamics of chromatin. In these experiments, 100 nM Trichostatin A (TSA), used as a representative histone deacetylase inhibitor, was added to coverslip-grown cells 3 h before measurement.

Test solution

To test the presented FRAP method in a simplest case of a homogeneous media without binding sites, the fluorescein isothiocyanate labeled human serum albumin (FITC-HSA, modification extent 1.5:1) was used in concentration of one micromole per liter in the glycerol/water mixture (80% w/w, phosphate-buffered saline buffer 0.05 M, pH 8). The content of glycerol in water is due to obtain the required range of diffusion coefficients. The sample volume of 5 μL was placed on sample glass covered with cover glass of 24 × 24 mm and sealed with paraffin. It yields the thickness of layer ~10 μm. The experiments have been carried out during 1 h after preparation.

FRAP protocol

FRAP experiments were performed on a Leica TCS SP5X (Leica, Wetzlar, Germany) confocal microscope with a 63×/1.4 NA oil immersion objective (pinhole diameter, 1 Airy; optical planar resolution, 0.17 μm; depth resolution, 0.5 μm). Cells were kept at 37°C and 5% CO_2 using an air-stream stage incubator (EMBL, Heidelberg, Germany). Bleaching was performed using a 30-mW argon-ion laser operating at 80% laser power at wavelengths of 476, 488, and 514 nm. A large area (approximately half a nucleus) was photobleached. Fluorescence recovery was monitored for 20 s at ~1-s intervals with a frame resolution of 512 × 512 pixels using a 40-mW White laser at low laser intensity (497 nm, 10% laser power).

THEORY

We assume that the diffusion of binding sites (and bound complexes) is neglected on the time- and length-scale of the FRAP measurement. This is a widely used approximation, for example, for FRAPs of cytoskeleton and DNA binding proteins where the binding sites are part of a large, relatively immobile complex (38–40). Also, we follow a conventional assumption that the intrinsic diffusion coefficient D of a free (unbound) protein is a constant (i.e., independent of spatial variables and time). Then the differential equations of two-dimensional diffusion with ligand-receptor type binding of target protein can be considered (40),

$$\begin{cases} \dfrac{\partial F}{\partial t} = D\dfrac{\partial^2 F}{\partial x^2} + D\dfrac{\partial^2 F}{\partial y^2} - k_+ AF + k_- B \\ \dfrac{\partial A}{\partial t} = -k_+ AF + k_- B \\ \dfrac{\partial B}{\partial t} = k_+ AF - k_- B \end{cases}, \qquad (1)$$

where x and y are spatial variables; t is time; F is the free (unbound) protein concentration; A is the vacant binding sites concentration; B is the bound protein (complexes) concentration; k_+ is the association rate constant; and k_- is the dissociation rate constant. We emphasize that, unlike conventional models of FRAP, the spatial distribution of binding sites in our model is considered to be inhomogeneous; that is, the concentration A is a function of spatial variables, as well as all other concentrations in Eq. 1. The observed fluorescence intensity at a certain spatial point (x,y) is proportional to the local sum of free and bound protein concentrations:

$$I(x,y,t) = F(x,y,t) + B(x,y,t).$$

It follows from Eq. 1 that

$$\frac{\partial I}{\partial t} = D\frac{\partial^2 F}{\partial x^2} + D\frac{\partial^2 F}{\partial y^2}. \quad (2)$$

Usually, Eq. 1 is simplified significantly by the assumption that the system has reached equilibrium before photobleaching (marked by a "b" subscript),

$$\begin{cases} 0 = -k_+ AF_b + k_- B_b \\ 0 = D\dfrac{\partial^2 F_b}{\partial x^2} + D\dfrac{\partial^2 F_b}{\partial y^2} \end{cases} \quad (3)$$

and both the spatial distribution of binding sites and the total amount of GFP fusion protein remain unchanged during the FRAP experiment. This is a reasonable and commonly applicable approximation since the typical duration of FRAP ranges from seconds to several minutes, whereas changes in GFP fusion protein expression in a cell occur over a time course of hours (40). Denoting the local equilibrium constant $K(x,y)$, as

$$K(x,y) = \frac{k_+ A(x,y)}{k_-}, \quad (4)$$

the following expression for the observed fluorescence intensity before bleaching is obtained from Eq. 3:

$$I_b(x,y) = F_b + B_b(x,y) = (1 + K(x,y))F_b. \quad (5)$$

It should be noted that the concentration of unbound protein before bleaching, F_b, does not depend on (x,y), because there is no change in the local concentration under stationary conditions ($\partial I_b(x,y,t)/\partial t = 0$).

The act of photobleaching converts some fluorescent protein molecules to nonfluorescent ones, but it does not alter the equilibrium for total (bleached plus unbleached) protein concentration. Therefore, the local concentration of vacant binding sites $A(x,y)$ remains unchanged on the timescale of the FRAP measurement. But the equilibrium for bleached and unbleached molecules is disturbed, and the return to the equilibrium concentration of the unbleached (i.e., fluorescent) protein is governed by Eq. 2. After bleaching, nonstationary conditions exist, which we consider in the context of the diffusion-dominant model (40).

The diffusion-dominant model is applied when the time of reaction equilibration on binding sites is much shorter than the time required to diffuse across the region of averaging the fluorescence intensity (ROI). Because the characteristic time of the binding-unbinding equilibration is $(k_- + k_+A)^{-1}$, and the characteristic time of the diffusion across the region of the size w is $(Dw^2)^{-1}$, the condition of the diffusion-dominant model is

$$(k_- + k_+ A)^{-1} \ll \left(Dw^2\right)^{-1}.$$

By increasing the size w of the ROI (which leads to an increase in the time required to diffuse across the region), the applicability of the diffusion model can be expanded to include a consideration of samples with slower binding rates. Thus, according to the diffusion-dominant model, the local equilibrium remains after bleaching,

$$0 = -k_+ A(x,y)F(x,y,t) + k_- B(x,y,t) \quad (6)$$

and therefore,

$$\begin{aligned} I(x,y,t) &= F(x,y,t) + B(x,y,t) \\ &= (1 + K(x,y))F(x,y,t). \end{aligned} \quad (7)$$

Taking into account Eqs. 5 and 7, Eq. 2 can be modified as

$$\frac{\partial}{\partial t} I(x,y,t) = F_b D\left(\frac{\partial^2}{\partial x^2} + \frac{\partial^2}{\partial y^2}\right)\tilde{I}(x,y,t), \quad (8)$$

where

$$\tilde{I}(x,y,t) = \frac{I(x,y,t)}{I_b(x,y)} = \frac{F(x,y,t)}{F_b}. \quad (9)$$

Inside of the frame, one can select a rectangular ROI, which may be different (in our method) from the ROB. Then, applying a sine-weighted integration (sine window transform) to Eq. 8 over spatial variables (x,y) in the range of the ROI ($0 < x < a$; $0 < y < b$) yields

$$\begin{aligned} &\int_0^a \sin\left(\frac{\pi x}{a}\right)dx \int_0^b \sin\left(\frac{\pi y}{b}\right)dy \left[\frac{\partial}{\partial t} I(x,y,t)\right] \\ &= \int_0^a \sin\left(\frac{\pi x}{a}\right)dx \int_0^b \sin\left(\frac{\pi y}{b}\right)dy \\ &\quad \left[F_b D\left(\frac{\partial^2}{\partial x^2} + \frac{\partial^2}{\partial y^2}\right)\tilde{I}(x,y,t)\right]. \end{aligned} \quad (10)$$

We should emphasize that the spatial frequency applied to the transform in Eq. 10 is lower (twofold) than the lowest spatial frequency of the Fourier method (34), and thus further reduces data processing noise. Applying the rules of integration by parts to the right side of Eq. 10 yields

$$\frac{1}{F_b D}\frac{\partial}{\partial t}\hat{\tilde{I}}(t) = -\pi^2\left(\frac{1}{b^2} + \frac{1}{a^2}\right)\hat{\tilde{I}}(t) + J(t), \quad (11)$$

where "$\hat{}$" under the function denotes the sine-weighted integration over the ROI, and the function $J(t)$ is defined by the ROI boundary values of $\tilde{I}(x,y,t)$:

$$\begin{aligned} J(t) &= \frac{\pi}{b}\int_0^a \sin\left(\frac{\pi x}{a}\right)\left[\tilde{I}(x,0,t) + \tilde{I}(x,b,t)\right]dx \\ &\quad + \frac{\pi}{a}\int_0^b \sin\left(\frac{\pi y}{b}\right)\left[\tilde{I}(0,y,t) + \tilde{I}(a,y,t)\right]dy. \end{aligned} \quad (12)$$

From Eq. 11, an averaged (over the ROI) effective diffusion coefficient can be obtained in the following manner.

The relation between mean I_b and mean K over the ROI follows from equation Eq. 5:

$$\begin{aligned}\overline{I}_b &= \frac{1}{ab}\int_0^b dy \int_0^a I_b(x,y)dx \\ &= \frac{F_b}{ab}\int_0^b dy \int_0^a (1 + K(x,y))dx = (1 + \overline{K})F_b.\end{aligned} \tag{13}$$

Taking into account Eq. 13, Eq. 11 can be rewritten in the form

$$\frac{\partial}{\partial t} G(t) = \frac{D}{1 + \overline{K}} S(t), \tag{14}$$

where

$$S(t) = -\pi^2\left(\frac{1}{b^2} + \frac{1}{a^2}\right)\hat{\tilde{I}}(t) + J(t) \tag{15}$$

and

$$G(t) = \frac{\hat{I}(t)}{\overline{I}_b}. \tag{16}$$

One can easily calculate experimental functions $S(t)$ and $G(t)$ directly from video-FRAP data. But one cannot obtain these functions theoretically, if the binding sites spatial distribution is unknown. Therefore, the commonly used fitting treatment of experimental curves by theoretical ones to obtain a desired parameter is impossible to apply in this case. Nevertheless, one can obtain the effective diffusion coefficient D_{eff}

$$D_{eff} = \frac{D}{1 + \overline{K}} \tag{17}$$

for unknown spatial distribution of binding sites by a treatment of the experimental functions $S(t)$ and $G(t)$ with the theoretical relation of Eq. 14. The main difficulty of the treatment comes from the data processing noise, which reduces the accuracy of the calculation of the derivative of the experimental function $G(t)$ on time. For the reduction of the experimental noise, one can apply the following two procedures:

1. Averaging the reference image $I_b(x,y)$ over a few video-frames before the bleach.
2. Low-pass, two-dimensional spatial filtering of the video-frames.

In addition, instead of the derivative calculation, we suggest the integration (that is more stable against the noise) of Eq. 14 over time (with a variable upper limit, p), which leads to the following equation for D_{eff}:

$$D_{eff} = \left[\int_0^p S(t)dt\right]^{-1}(G(p) - G(0)). \tag{18}$$

A particular feature of the method is that D_{eff} is averaged over the rectangular ROI chosen by the researcher. On the other hand, one may have an idea to obtain D_{eff} averaged over a cell nucleus, which is not rectangular. This is possible, if the equilibrium constant $K(x,y)$ is much greater inside the nucleus than outside. This situation is indicated by the fluorescence intensity distribution of the reference frame before the bleach: the fluorescence intensity is much greater inside the nucleus than outside. In this situation one can chose the rectangular ROI that enclose the whole nucleus and then carry out the following correction of the obtained D_{eff} (averaged over the ROI). Selecting a background level between the low fluorescence intensity outside and the high fluorescence intensity inside the nucleus one counts the number of pixels in the ROI with the intensity above the level.

The ratio of this number to the total number of pixels of the ROI (i.e., the ratio of the areas of the nucleus and the ROI) is the correction factor. According to Eqs. 13 and 17, the correction factor has to be multiplied to D_{eff} to obtain the average effective diffusion coefficient of the whole nucleus. This correction procedure of the data obtained with Eq. 18 was used in this work to process experimental video-FRAP data measured by laser-scanning confocal microscopy. To reduce the noise, the reference image $I_b(x,y)$ was averaged over 20 video-frames before the bleach. In addition, a spatial nonweighted averaging over 16 (four pixels in each dimension) neighboring pixels of a video frame was applied as the two-dimensional spatial filtering method. The number of frames, p, in data processing was varied to estimate the error of D_{eff} as the standard deviation of the $D_{eff}(p)$ array.

RESULTS AND DISCUSSION

Test of the method on a cell nucleus

The test was carried out to verify a general applicability of the method for FRAP investigations of a cell nucleus. As an example, the dynamics of GFP-HP1β in a nucleus of a living *Suv39h*$^{+/+}$ mouse embryonic fibroblast was measured. We have to mention that proteins HP1α, HP1β, and HP1γ are very similar, so the justification only for HP1β was demonstrated in Figs. 1–3 of the article. To increase the signal/noise ratio, a large area (approximately one-half of a nucleus) of the ROB was applied, as illustrated on Fig. 1 *A*.

Taking into account the known literature (41) values for this system (HP1 in MEF nuclei)—D ~24 μm^2/s, k_+A ~1.7 s^{-1}, and k_- ~0.6 s^{-1}—it is possible to theoretically estimate (by the expression $(k_- + k_+A)^{-1} << (Dw^2)^{-1}$) that the diffusion-dominant model is applicable, if the size of the ROI is >3 μm. The applicability of the two-dimensional diffusion model of Eq. 1 (instead of the complete three-dimensional diffusion treatment) was experimentally verified by monitoring the temporal variation in total intensity over the entire image. Fig. 1 *B* shows that the total amount of fluorescence in the sample after bleaching is

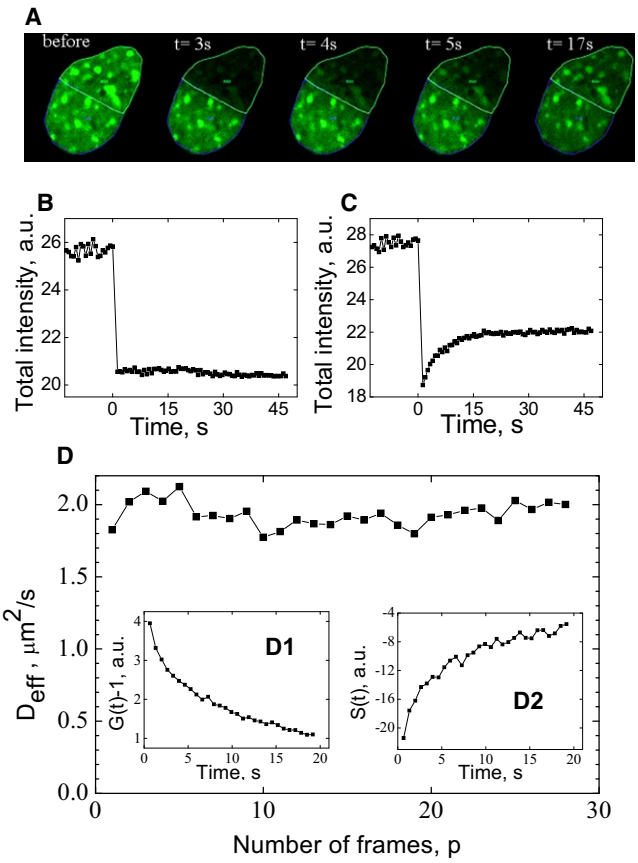

FIGURE 1 (*A*) FRAP experiments for the analysis of chromatin-binding proteins; GFP-tagged HP1β proteins in MEF cells were imaged before and during recovery after bleaching of about half the nuclear area; images were taken at the indicated times (t) after the end of the bleach pulse. (*B*) Illustration of typical intensity variations before and after bleaching ($t = 0$ s), where the total intensity is the sum over the entire image (the data obtained during bleaching have been omitted). (*C*) Illustration of typical intensity variations before and after bleaching (t = 0 s), where the total intensity is the sum over the bleach area of the image (the data obtained during bleaching have been omitted). (*D*) Evaluation of D_{eff} as a function of the number of frames taken after bleaching in the case of the coincidence of the rectangular ROI with the video-frame (the correction on the background pixels number is applied). (*Inset D*1) Experimental curve of $G(t)$. (*Inset D*2) Experimental curve of $S(t)$.

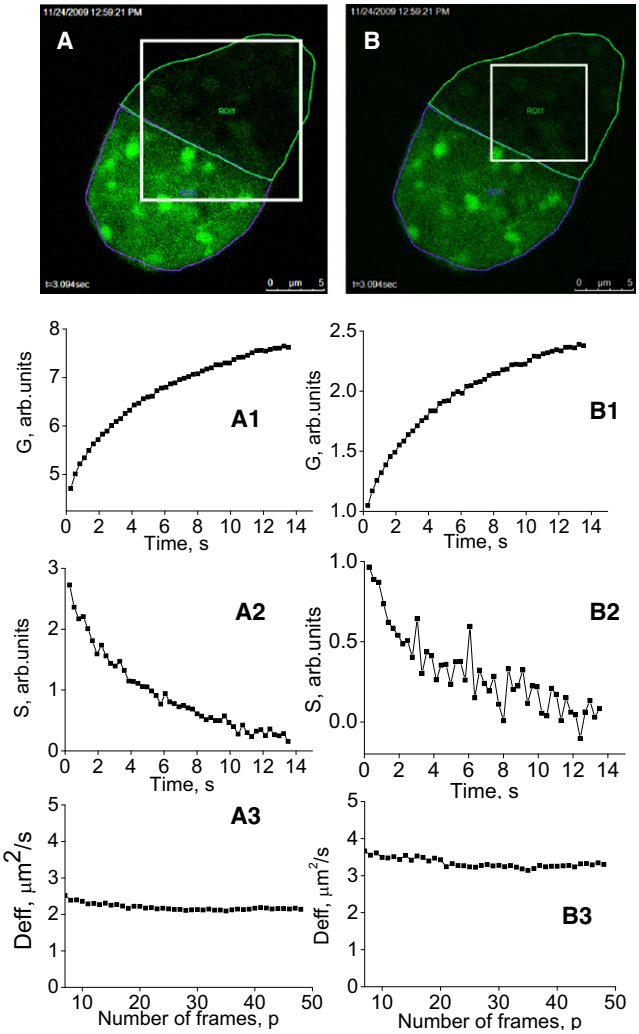

FIGURE 2 Evaluation of D_{eff} as a function of the number of frames taken after bleaching in the case of the ROI (*white solid rectangular contour*) smaller than the video-frame (the correction on the background pixels number is applied). (*A*) The ROI is partially inside of the nucleus. (*B*) The ROI is completely inside of the nucleus. (*A*1,*B*1) Corresponding experimental curves of $G(t)$. (*A*2,*B*2) Corresponding experimental curves of $S(t)$. (*A*3,*B*3) Corresponding evaluation of D_{eff} as a function of the number of frames taken after bleaching.

a constant (within the noise), supporting the assumption that the net influx of molecules from outside the field of view is negligible compared to the observed fluorescence recovery presented in Fig. 1 *C*.

Fig. 1 illustrates the case when the rectangular ROI coincided with the whole video-frame. The effective diffusion coefficient D_{eff} plotted against the number of frames required for the evaluation after bleaching is presented on Fig. 1 *D*. The corresponding experimental curves of the functions $G(t)$ and $S(t)$ are shown in the insets D1 and D2 of Fig. 1 *D*. The variation in the effective diffusion coefficient as a function of the number of frames taken allows one to estimate the standard error of D_{eff}. The two examples of the treatment of the same experimental data using the rectangular ROI smaller than the whole frame are presented on Fig. 2. The test was successful: the obtained D_{eff} is in good agreement with known literature data (41) on the same system (HP1 in mouse embryonic fibroblasts nuclei).

Test on FITC-HSA in glycerol/water mixture

We tested the method in the simplest case of homogeneous media without binding sites ($K(x,y) = 0$) in order to compare the obtained diffusion coefficient with known literature data (obtained by well-established existing approaches). The experiments were carried out at $T = 30$°C. Three different bleaching regions (ROB) were applied for the experiments on photobleaching FITC-HAS molecules in

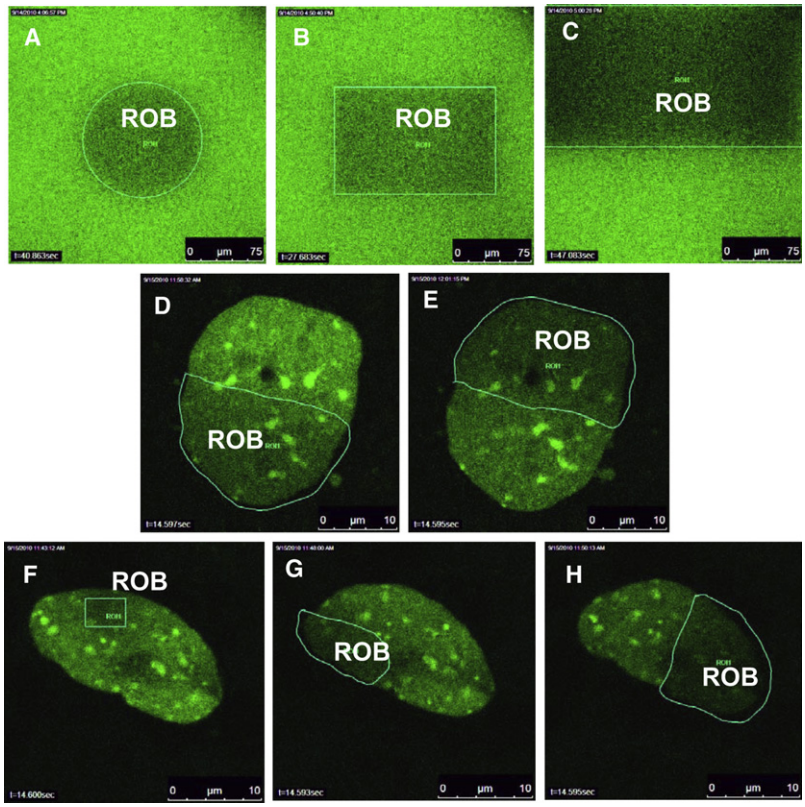

FIGURE 3 (*A–C*) FRAP test on pure diffusion measurement of FITC-HSA in the glycerol/water homogeneous mixture without binding sites using different bleaching regions (ROB) in the case of the coincidence of the rectangular ROI with the video-frame. (*D* and *E*) The FRAP test on D_{eff} measurement of the GFP-labeled protein in a cell nucleus using different positions of the ROB. (*F–H*) The FRAP test on D_{eff} measurement of the GFP-labeled protein in a cell nucleus using different sizes of the ROB.

the glycerol/water mixture in the case of the coincidence of the rectangular ROI with the video-frame, as shown on Fig. 3, *A–C*. As the result, we observed a good agreement (Table 1) of the obtained diffusion coefficients with the known literature data (42) recalculated for $T = 30°C$, taking into account the temperature dependence of the diffusion coefficient (43).

Test on GFP-HP1 in a cell nucleus using different positions of bleaching area

The test is to verify experimentally the independence (within noise) of the obtained D_{eff} on the bleaching region (ROB) position in an inhomogeneous cell nucleus in the case of the coincidence of the rectangular ROI with the video-frame, as illustrated on Fig. 3, *D* and *E*. The experiments were carried out consequently with the same cell nucleus. The obtained D_{eff} are presented in Table 2. One can see that the variation of D_{eff} due to different positions of the ROB is within the error of the evaluation and is in good agreement with known literature data (41) for the same system.

Test on GFP-HP1 in a cell nucleus using different sizes of bleaching area

The test is to verify experimentally the independence (within noise) of the obtained D_{eff} on the bleaching region (ROB) size in an inhomogeneous cell nucleus in the case of the coincidence of the rectangular ROI with the video-frame, as illustrated on Fig. 3, *F–H*. The experiments were carried out consequently with the same cell nucleus. The obtained data on D_{eff} are presented in Table 2. One can see that the variation of D_{eff} due to different sizes of the ROB is within the error of

TABLE 1 Diffusion coefficient of FITC-HSA molecules in the glycerol/water mixture (80% w/w, phosphate-buffered saline buffer 0.05 M, pH 8) obtained in our FRAP experiments at different bleaching areas (ROB) in the case of the coincidence of the rectangular ROI with the video-frame

	Results of this work			
FITC-HSA glycerol/water	A	B	C	Known literature data recalculated for $T = 30°C$ using Saltzman et al. (42) and Phiilles et al. (43)
D, $\mu m^2/s$	4.2 ± 1.5	5.4 ± 1.4	3.7 ± 1.0	2.2 ± 0.5

Data as illustrated in Fig. 3, *A–C*, and the known literature data recalculated for $T = 30°C$. Relatively big error of the obtained values is due to a low signal/noise ratio in the video-FRAP experiments.

TABLE 2 Effective diffusion coefficient of GFP-labeled protein in a cell nucleus obtained with different positions and sizes of ROB in the case of the coincidence of the rectangular ROI with the video-frame (the correction on the background pixels number is applied)

	Experimental results of this work					
GFP-HP1β MEF-wt	D	E	F	G	H	Muller et al. (41)
D_{eff}, $\mu m^2/s$	2.1 ± 0.7	3.3 ± 1.1	3.7 ± 1.0	5.4 ± 1.2	5.2 ± 1.1	2.3 ± 0.4

Data as illustrated in Fig. 3, *D–H*, and the known literature data (41).

the evaluation and is in good agreement with known literature data (41) for the same system.

Application to intranuclear diffusion

We applied the method described above to the FRAP investigation of HP1 (α, β, γ) dynamics in nuclei of living cells (Fig. 4, *A* and *B*) in the case of the coincidence of the rectangular ROI with the video-frame. MEFs from *Suv39h1/2*$^{-/-}$ and *Lmna*$^{-/-}$ mice, and their corresponding wt mice were transfected with HP1-GFP (HP1α, HP1β, and HP1γ) and evaluated using our experimental protocol for FRAP. These studies were also supplemented by experiments analyzing the influence of histone deacetylase inhibition on the structure and dynamics of chromatin, using TSA as a representative inhibitor of histone deacetylases.

To measure HP1 dynamics in the nuclei of living cells, we screened different MEF cell lines exogenously expressing GFP fusion proteins of different HP1 isoforms. The big standard mean error of the effective diffusion coefficients for different cell populations presented on Fig. 4, *A* and *B*, are due to a relatively small number of cells obtained for the analysis. An analysis of diffusion coefficients showed differences among the three HP1 subtypes, some of which were dependent on histone methyltransferases.

In *Suv39h1/2*$^{-/-}$ MEFs, the diffusion of HP1α was low relative to that of HP1β and HP1γ, indicating that a deficiency of histone methyltransferases Suv39h1 and Suv39h2 (verified by Harničarová Horáková et al. (44)) reduced the diffusibility of HP1γ, but not HP1α or HP1β. Additionally, after TSA treatment, the diffusion coefficients decreased for HP1α and HP1γ, but increased for HP1β. These data confirmed our suggestion based on previous experiments that TSA treatment differentially affects the biological features of HP1β compared with HP1α and HP1γ (45,46).

It should also be noted that GFP-HP1 was largely lost from heterochromatic foci, termed chromocenters (47), in *Suv39h1/2*$^{-/-}$ cells, and FRAP analyses showed an overall increase in the mobility of fusion proteins in these cells compared with that in control *Suv39h*$^{+/+}$ cells. As reported by Cheutin et al. (47), the mobility of HP1 proteins in heterochromatin reflects their binding to target sites created by SUV39h HMTs. Moreover, data presented by Cheutin et al. (47) confirmed the fundamental role of SUV39h HMTs in HP1 binding and diffusion in vivo. In *Lmna*$^{-/-}$ cells, the diffusion coefficients for HP1α and HP1β were significantly different after TSA treatment, which remarkably increased the diffusion of both HP1α and HP1β subtypes. These results confirm the correlation between LMNA deficiency and nuclear distribution of HP1 subtypes previously reported by Scaffidi and Misteli (48) and Shumaker et al. (49).

Taken together, our results demonstrate that both TSA treatment and LMNA deficiency influence the diffusibility of HP1 proteins. One can see this from Fig. 4, *A* and *B*, which shows rather large error bars. Alathough this reduced statistical power limits our ability to answer certain biological questions (e.g., what is the basis for differences in the

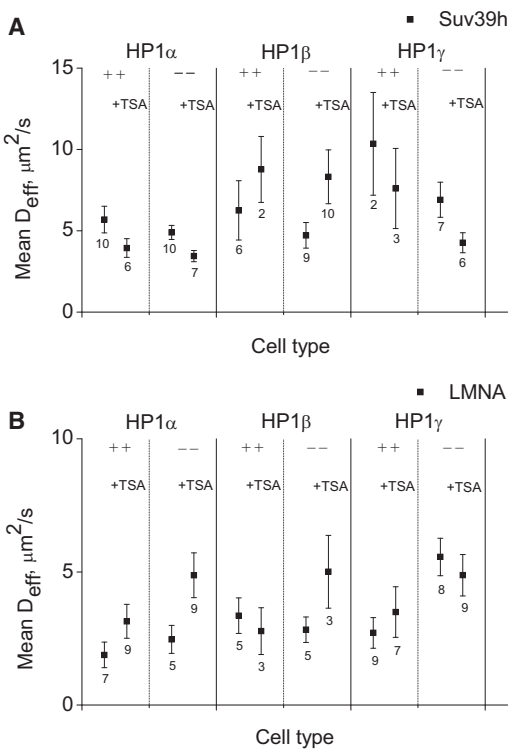

FIGURE 4 Results of the application of the method for the FRAP investigation of HP1 (α, β, γ) dynamics in nuclei of living cells in the case of the coincidence of the rectangular ROI with the video-frame (the correction on the background pixels number is applied). Means (*dots*) and standard mean errors (*error bars*) of the effective diffusion coefficients measured for different isoforms of HP1 in Suv39h (*A*) and Lmna (*B*) cell populations: ++, wt cells; –, *Suv39h1/2*-deficient (*A*) or *Lmna*-deficient (*B*) cells. *+TSA* represents cells after Trichostatin A treatment. Numbers under the dots signify the number of cells treated.

mobility of different HP1 isoforms? How are mobilities influenced by SUV39h and LMNA deficiencies or TSA-mediated histone hyperacetylation?) it does not affect our intended purpose of validating the application of this new (to our knowledge) method, which is amply illustrated by our results.

Advantages of the proposed FRAP analysis

In our view, the key advantage of this method is that it provides a quantitative evaluation of protein mobility (effective diffusion coefficient) in inhomogeneous media in the presence of binding of target molecules using FRAP techniques, without requiring a mathematical solution of master diffusion-reaction equations. The much larger ROI allows one to extend the effective diffusion approach to much slower reactions that cannot be treated with the diffusion-dominant scenario using conventional FRAP methods using a small fluorescence intensity averaging area (spot).

The method is most useful for the investigation of highly inhomogeneous areas, such as cell nuclei, where a mathematical solution of master diffusion-reaction equations is practically unachievable due to insufficient structural information. The method is independent of the bleached area geometry, the bleach laser-beam profile, the spatial distribution of binding sites, and the position of the cell nucleus in the frame of treatment. Therefore, it can easily be adapted, for example, to automatic single-cell FRAP measurements, collected at rates of hundreds of cells per hour, to yield robust statistics.

Prospects for further improvement in quantitative FRAP

There are a few limitations of the method. The most significant limitation is that the association and the dissociation rate constants are not evaluated independently; instead, the ratio of these values in the form of an equilibrium constant can be estimated from the effective diffusion coefficient. Another limitation is that the method can be applied only within the diffusion-dominant scenario (although the ROI area is increased significantly, expanding the applicability of the effective diffusion model to slower binding reactions).

This method also has limitations in common with conventional FRAP (32,36): cells are not changed or moved during FRAP experiments; the intrinsic diffusion coefficient D is a constant (i.e., independent of spatial variables and time); the diffusion of binding sites is neglected; etc. We anticipate that further development of the method should overcome as least some of these limitations.

CONCLUSIONS

What to our knowledge is a new approach has been developed for determining effective diffusion of proteins in inhomogeneous media. The approach is based on GFP technology, spatial measurements using a video-FRAP technique, advanced laser-scanning confocal microscopy, and analysis of results by means of a mathematical model that reflects the real situation in many cases.

We believe the method described here will expand the range of applications of quantitative FRAP analysis in inhomogeneous media, and provide greater and more accurate insight into the biological processes underlying FRAP recovery. Our method was successfully applied to intranuclear diffusion measurements in living cells expressing HP1-GFP. The obtained D_{eff} is in a reasonable agreement with known literature data on similar systems. Considering the ease-of-use of this method, we expect that it will make quantitative measurements of diffusion much more accessible to researchers in the life sciences.

We thank Prof. Thomas Jenuwein and Dr. Suzane Opravil for providing us the *Suv39h*-deficient cells and relevant controls. GFP-HP1 (α, β, γ) plasmids were a generous gift from Dr. Tom Misteli, Laboratory of Receptor Biology and Gene Expression, National Institute of Health (Bethesda, MD). We are also grateful to Dr. Yuri I. Glazachev from ICKC (Novosibirsk, Russia) for valuable discussions and to BioScience Writers (Houston, TX) for the linguistic revision of our manuscript.

This work was supported by research project Nos. LC535, ME919, AVOZ50040702, and AVOZ50040507; integration grants from the Siberian Branch of the Russian Academy of Science, Nos. 2009-37 and 2009-7; a grant from the program of the Presidium of the Russian Academy of Science, No. 2009-27-15; and by programs of the Russian Ministry of Education and Science (contract Nos. P422, P2497, P1039, and 14-740-11-0729). This work also has been supported by Marie Curie grant PIRSES-GA-2010-269156-LCS, and by Grant Agency of Czech Republic (grant P302/10/1022).

REFERENCES

1. Sprague, B. L., and J. G. McNally. 2005. FRAP analysis of binding: proper and fitting. *Trends Cell Biol.* 15:84–91.
2. Festenstein, R., S. N. Pagakis, …, D. Kioussis. 2003. Modulation of heterochromatin protein 1 dynamics in primary mammalian cells. *Science.* 299:719–721.
3. Dundr, M., U. Hoffmann-Rohrer, …, T. Misteli. 2002. A kinetic framework for a mammalian RNA polymerase in vivo. *Science.* 298:1623–1626.
4. Shav-Tal, Y., X. Darzacq, …, R. H. Singer. 2004. Dynamics of single mRNPs in nuclei of living cells. *Science.* 304:1797–1800.
5. Elsner, M., H. Hashimoto, …, M. Weiss. 2003. Spatiotemporal dynamics of the COPI vesicle machinery. *EMBO Rep.* 4:1000–1004.
6. Giese, B., C. K. Au-Yeung, …, G. Müller-Newen. 2003. Long term association of the cytokine receptor gp130 and the Janus kinase Jak1 revealed by FRAP analysis. *J. Biol. Chem.* 278:39205–39213.
7. Shaw, S. L., R. Kamyar, and D. W. Ehrhardt. 2003. Sustained microtubule treadmilling in *Arabidopsis* cortical arrays. *Science.* 300:1715–1718.
8. Smith, A. J., J. R. Pfeiffer, …, B. S. Wilson. 2003. Microtubule-dependent transport of secretory vesicles in RBL-2H3 cells. *Traffic.* 4: 302–312.
9. von Wichert, G., B. Haimovich, …, M. P. Sheetz. 2003. Force-dependent integrin–cytoskeleton linkage formation requires downregulation of focal complex dynamics by Shp2. *EMBO J.* 22:5023–5035.
10. Howell, B. J., B. Moree, …, E. Salmon. 2004. Spindle checkpoint protein dynamics at kinetochores in living cells. *Curr. Biol.* 14:953–964.

11. Peters, R., J. Peters, …, W. Bähr. 1974. A microfluorimetric study of translational diffusion in erythrocyte membranes. *Biochim. Biophys. Acta.* 367:282–294.
12. Axelrod, D., D. E. Koppel, …, W. W. Webb. 1976. Mobility measurement by analysis of fluorescence photobleaching recovery kinetics. *Biophys. J.* 16:1055–1069.
13. Koppel, D. E., D. Axelrod, …, W. W. Webb. 1976. Dynamics of fluorescence marker concentration as a probe of mobility. *Biophys. J.* 16:1315–1329.
14. Cole, N. B., C. L. Smith, …, J. Lippincott-Schwartz. 1996. Diffusional mobility of Golgi proteins in membranes of living cells. *Science.* 273:797–801.
15. Swaminathan, R., C. P. Hoang, and A. S. Verkman. 1997. Photobleaching recovery and anisotropy decay of green fluorescent protein GFP-S65T in solution and cells: cytoplasmic viscosity probed by green fluorescent protein translational and rotational diffusion. *Biophys. J.* 72:1900–1907.
16. Patterson, G. H., S. M. Knobel, …, D. W. Piston. 1997. Use of the green fluorescent protein and its mutants in quantitative fluorescence microscopy. *Biophys. J.* 73:2782–2790.
17. Partikian, A., B. Olveczky, …, A. S. Verkman. 1998. Rapid diffusion of green fluorescent protein in the mitochondrial matrix. *J. Cell. Biol.* 140:821–829.
18. Adams, C. L., Y.-T. Chen, …, W. J. Nelson. 1998. Mechanisms of epithelial cell-cell adhesion and cell compaction revealed by high-resolution tracking of E-cadherin-green fluorescent protein. *J. Cell. Biol.* 142:1105–1119.
19. Houtsmuller, A. B., and W. Vermeulen. 2001. Macromolecular dynamics in living cell nuclei revealed by fluorescence redistribution after photobleaching. *Histochem. Cell. Biol.* 115:13–21.
20. Scholz, M., C. Gross-Johannböcke, and R. Peters. 1988. Measurement of nucleocytoplasmic transport by fluorescence microphotolysis and laser scanning microscopy. *Cell. Biol. Int. Rep.* 12, 709–27.
21. Tsibidis, G. D., and J. Ripoll. 2008. Investigation of binding mechanisms of nuclear proteins using confocal scanning laser microscopy and FRAP. *J. Theor. Biol.* 253:755–768.
22. Kao, H. P., J. R. Abney, and A. S. Verkman. 1993. Determinants of the translational mobility of a small solute in cell cytoplasm. *J. Cell Biol.* 120:175–184.
23. Verkman, A. S. 2003. Diffusion in cells measured by fluorescence recovery after photobleaching. *In* Biophotonics, Part A: Methods in Enzymology, Vol. 360. G. Marriott and I. Parker, editors. Academic Press, New York. 635–648.
24. Bjarneson, D. W., and N. O. Petersen. 1991. Effects of second order photobleaching on recovered diffusion parameters from fluorescence photobleaching recovery. *Biophys. J.* 60:1128–1131.
25. Blonk, J. C. G., A. Don, …, J. J. Birmingham. 1993. Fluorescence photobleaching recovery in the confocal scanning light microscope. *J. Microsc.* 169:363–374.
26. Braeckmans, K., L. Peeters, …, J. Demeester. 2003. Three-dimensional fluorescence recovery after photobleaching with the confocal microscope. *Biophys. J.* 85:2240–2252.
27. Lopez, A., L. Dupou, …, J. Tocanne. 1988. Fluorescence recovery after photobleaching (FRAP) experiments under conditions of uniform disk illumination. *Biophys. J.* 53:963–970.
28. Wedekind, P., U. Kubitscheck, …, R. Peters. 1996. Line-scanning microphotolysis for diffraction-limited measurements of lateral diffusion. *Biophys. J.* 71:1621–1632.
29. Kubitscheck, U., P. Wedekind, and R. Peters. 1998. Three-dimensional diffusion measurements by scanning microphotolysis. *J. Microsc.* 192:126–138.
30. Periasamy, N., and A. S. Verkman. 1998. Analysis of fluorophore diffusion by continuous distributions of diffusion coefficients: application to photobleaching measurements of multicomponent and anomalous diffusion. *Biophys. J.* 75:557–567.
31. Wachsmuth, M., T. Weidemann, …, J. Langowski. 2003. Analyzing intracellular binding and diffusion with continuous fluorescence photobleaching. *Biophys. J.* 84:3353–3363.
32. Lele, T. P., and D. E. Ingber. 2006. A mathematical model to determine molecular kinetic rate constants under non-steady state conditions using fluorescence recovery after photobleaching (FRAP). *Biophys. Chem.* 120:32–35.
33. Kang, M., and A. K. Kenworthy. 2008. A closed-form analytic expression for FRAP formula for the binding diffusion model. *Biophys. J.* 95:L13–L15.
34. Tsay, T., and K. A. Jacobson. 1991. Spatial Fourier analysis of video photobleaching measurements, principles and optimization. *Biophys. J.* 60:360–368.
35. Berk, D. A., F. Yuan, …, R. K. Jain. 1993. Fluorescence photobleaching with spatial Fourier analysis: measurement of diffusion in light-scattering media. *Biophys. J.* 65:2428–2436.
36. Mueller, F., P. Wach, and J. G. McNally. 2008. Evidence for a common mode of transcription factor interaction with chromatin as revealed by improved quantitative fluorescence recovery after photobleaching. *Biophys. J.* 94:3323–3339.
37. Jonsson, P., M. P. Jonsson, …, F. Hook. 2008. A method improving the accuracy of fluorescence recovery after photobleaching analysis. *Biophys. J.* 95:5334–5348.
38. Bulinski, J. C., D. J. Odde, …, C. M. Waterman-Storer. 2001. Rapid dynamics of the microtubule binding of ensconsin in vivo. *J. Cell Sci.* 114:3885–3897.
39. Coscoy, S., F. Waharte, …, F. Amblard. 2002. Molecular analysis of microscopic ezrin dynamics by two-photon FRAP. *Proc. Natl. Acad. Sci. USA.* 99:12813–12818.
40. Sprague, B. L., R. L. Pego, …, J. G. McNally. 2004. Analysis of binding reactions by fluorescence recovery after photobleaching. *Biophys. J.* 86:3473–3495.
41. Muller, K. P., F. Erdel, …, K. Rippe. 2009. Multiscale analysis of dynamics and interactions of heterochromatin protein 1 by fluorescence fluctuation microscopy. *Biophys. J.* 97:2876–2885.
42. Saltzman, W. M., M. L. Radomsky, …, R. A. Cone. 1994. Antibody diffusion in human cervical mucus. *Biophys. J.* 66:508–515.
43. Phiilles, G. D. J. 1981. Translational diffusion coefficient of macroparticles in solvents of high viscosity. *J. Phys. Chem.* 85:2838–2843.
44. Harnicarová Horáková, A., G. Galiová, …, E. Bártová. 2010. Chromocenter integrity and epigenetic marks. *J. Struct. Biol.* 169, 124–33.
45. Bártová, E., J. Pacherník, …, S. Kozubek. 2005. Nuclear levels and patterns of histone H3 modification and HP1 proteins after inhibition of histone deacetylases. *J. Cell Sci.* 118:5035–5046.
46. Bártová, E., J. Pacherník, …, S. Kozubek. 2007. Differentiation-specific association of HP1 α and HP1 β with chromocenters is correlated with clustering of TIF1 β at these sites. *Histochem Cell Biol.* 127:375–388.
47. Cheutin, T., A. J. McNairn, …, T. Misteli. 2003. Maintenance of stable heterochromatin domains by dynamic HP1 binding. *Science.* 299: 721–723.
48. Scaffidi, P., and T. Misteli. 2006. Lamin A-dependent nuclear defects in human aging. *Science.* 312:1059–1063.
49. Shumaker, D. K., T. Dechat, …, R. D. Goldman. 2006. Mutant nuclear lamin A leads to progressive alterations of epigenetic control in premature aging. *Proc. Natl. Acad. Sci. USA.* 103:8703–8708.